Analysis of adiabatic shear bands in elasto-thermo-viscoplastic materials by modified smoothed-particle hydrodynamics (MSPH) method

R.C. Batra *, G.M. Zhang

Department of Engineering Science and Mechanics, MC 0219, Virginia Polytechnic Institute and State University, Blacksburg, VA 24061, USA

Abstract

We use the modified smoothed-particle hydrodynamics (MSPH) method to analyze shear strain localization in elasto-thermo-viscoplastic materials that exhibit strain- and strain-rate hardening and thermal softening. A homogeneous solution of simple shearing deformations of the body is perturbed and the resulting initial-boundary-value problem analyzed by the MSPH method. It is found that the deformation localizes into a narrow region of intense plastic deformation. In materials exhibiting enhanced thermal softening, an elastic unloading shear wave emanates from this region and propagates outwards. The time when the deformation localizes decreases exponentially with an increase in the thermal softening coefficient. Results have been computed without adding an artificial viscosity and compared with those obtained by the finite element method.
© 2004 Elsevier Inc. All rights reserved.

Keywords: Shear strain localization; Meshless method; Nonlinear problem

1. Introduction

The finite element method (FEM) has often been used to analyze nonlinear initial-boundary-value problems. For finite deformation problems involving either localization of deformation into thin narrow regions or failure or both, one needs to adaptively refine the FE mesh since otherwise the solution ceases because of severe distortion of one or more elements. The transfer of data from the old FE mesh to the

newly created nodes generally smoothes out the deformation field thereby either delaying the onset of localization or increasing the width of the localized region or both. One way to overcome these difficulties is to use a meshless method in which no nodal connectivity is needed and there are no elements that can be severely deformed. Two recent books [1,2] have summarized several meshless methods. However, these methods have not been widely applied to shear strain localization problems in which plastic deformations of a small region are significantly more than that of the rest of the material. This narrow region of intense plastic deformation is called an adiabatic shear band (ASB) since there is usually not enough time for the heat to be conducted away. However, thermal conductivity plays a significant role during the post-localization process. The study of ASBs is important because they precede ductile fracture in many metals deformed at high strain rates. Our ultimate goal is to analyze two- and three-dimensional shear strain localization problems by a meshless method. Here we use the modified smoothed-particle hydrodynamics (MSPH) method to analyze simple shearing deformations of an elasto-thermo-viscoplastic material and show that it captures well the localization of deformation and the emanation of an elastic unloading wave from the shear banded region. The problem was analyzed earlier by Batra [3], and Batra and Kim [4] with the FEM. Results computed with the MSPH method without adding any artificial viscosity are found to agree well with the FE solution and also with those obtained by the finite-difference method (FDM).

The SPH method is total Lagrangian and is due to Lucy [5] and Gingold and Monaghan [6]. It has been applied by Libersky and Petschek [7] to analyze finite deformations of an elastoplastic body. However, they ignored strain- and strain-rate hardening and thermal softening effects and therefore could not consider the localization of deformation into narrow regions of intense plastic deformation. Also they used the classical SPH method and we employ the MSPH method described below.

The conventional SPH method has two drawbacks: boundary deficiency and tensile instability. The boundary deficiency refers to the basis functions not satisfying the consistency condition at points near the boundaries. Chen et al. [8,9] applied the concept of the kernel estimate to the Taylor series expansion of a function and named it the corrective smoothed-particle method (CSPM); they have also summarized other pertinent literature. The CSPM took care of the latter problem but not the former one. Recently, techniques to further improve the tension instability and the zero energy modes have been proposed [10,11]. Zhang and Batra [12] modified the CSPM to improve upon the consistency condition, named it the MSPH and applied it to study one-dimensional wave propagation in an elastic bar and two-dimensional transient heat conduction in a plate. Here we use it to analyze coupled thermomechanical deformations of an elasto-thermo-viscoplastic body deformed in simple shear and delineate the localization of deformation into a narrow region. For materials exhibiting high thermal softening, the stress drops very rapidly at points within the region of localization and an elastic unloading wave emanates outwards and propagates with the speed of the elastic shear wave. The computed shear wave speed matches well with the analytical value. Also, width of the region of localized deformation agrees well with that found earlier by the FEM and with that observed experimentally [13].

The paper is organized as follows. The MSPH method is briefly reviewed in Section 2. Equations governing simple shearing deformations of a thermo-elasto-viscoplastic body, and the pertinent initial and boundary conditions are described in Section 3.1. A converged solution of these equations obtained by the FEM is taken as the reference solution. Errors in the numerical solution computed with the MSPH method are described in Section 3.2, and the decrease in error with an increase in the number of particles is delineated. The effect of the smoothing length in the MSPH kernel is described in Section 3.3. It is stated in Section 3.4 that the modified quartic spline kernel function did not yield good results. The post-localization response is discussed in Section 3.5. Section 3.6 compares numerical solutions obtained by the MSPH, FE and a pseudo-spectral method [15]. The MSPH and the FE methods are compared in Section 3.7, and conclusions are listed in Section 4.

2. The MSPH method

The Taylor series expansion of a scalar-valued function $f(\mathbf{x})$ about the point $\mathbf{x}^{(i)} = (x_1^{(i)}, x_2^{(i)}, x_3^{(i)}) = (x^{(i)}, y^{(i)}, z^{(i)})$ in a three-dimensional space is

$$f(\boldsymbol{\xi}) = f(\mathbf{x}^{(i)}) + \frac{\partial f}{\partial x_\alpha^{(i)}}(\xi_\alpha - x_\alpha^{(i)}) + \frac{1}{2}\frac{\partial^2 f}{\partial x_\alpha^{(i)}\partial x_\beta^{(i)}}(\xi_\alpha - x_\alpha^{(i)})(\xi_\beta - x_\beta^{(i)}) + \cdots, \tag{2.1}$$

where a repeated index implies summation over the range of the index; however, an index enclosed in parentheses is not summed. Multiplying both sides of Eq. (2.1) with a kernel function $W(\mathbf{x} - \boldsymbol{\xi}, h)$, the first derivative $W_\gamma = \partial W/\partial \xi_\gamma$ of the kernel function, the second derivative $W_{\gamma\delta} = \partial^2 W/\partial \xi_\gamma \partial \xi_\delta$ of the kernel function, neglecting the third and higher derivative terms, and integrating the resulting equations over the domain Ω, we obtain

$$\int_\Omega f(\boldsymbol{\xi}) W \, \mathrm{d}\boldsymbol{\xi} \simeq f_i \int_\Omega W \, \mathrm{d}\boldsymbol{\xi} + f_{\alpha i} \int_\Omega (\xi_\alpha - x_\alpha^{(i)}) W \, \mathrm{d}\boldsymbol{\xi} + \frac{1}{2} f_{\alpha\beta i} \int_\Omega (\xi_\alpha - x_\alpha^{(i)})(\xi_\beta - x_\beta^{(i)}) W \, \mathrm{d}\boldsymbol{\xi}, \tag{2.2}$$

$$\int_\Omega f(\boldsymbol{\xi}) W_\gamma \, \mathrm{d}\boldsymbol{\xi} \simeq f_i \int_\Omega W_\gamma \, \mathrm{d}\boldsymbol{\xi} + f_{\alpha i} \int_\Omega (\xi_\alpha - x_\alpha^{(i)}) W_\gamma \, \mathrm{d}\boldsymbol{\xi} + \frac{1}{2} f_{\alpha\beta i} \int_\Omega (\xi_\alpha - x_\alpha^{(i)})(\xi_\beta - x_\beta^{(i)}) W_\gamma \, \mathrm{d}\boldsymbol{\xi}, \tag{2.3}$$

$$\int_\Omega f(\boldsymbol{\xi}) W_{\gamma\delta} \, \mathrm{d}\boldsymbol{\xi} \simeq f_i \int_\Omega W_{\gamma\delta} \, \mathrm{d}\boldsymbol{\xi} + f_{\alpha i} \int_\Omega (\xi_\alpha - x_\alpha^{(i)}) W_{\gamma\delta} \, \mathrm{d}\boldsymbol{\xi} + \frac{1}{2} f_{\alpha\beta i} \int_\Omega (\xi_\alpha - x_\alpha^{(i)})(\xi_\beta - x_\beta^{(i)}) W_{\gamma\delta} \, \mathrm{d}\boldsymbol{\xi}, \tag{2.4}$$

where $f_i = f(\mathbf{x}^i)$, $f_{\alpha i} = \partial f/\partial x_\alpha^{(i)}$ and $f_{\alpha\beta i} = \partial^2 f/\partial x_\alpha^{(i)}\partial x_\beta^{(i)}$. Note that the kernel function involves the smoothing parameter h whose value affects the accuracy of the approximate solution; h determines the support of the kernel function. In order to simplify the notation, we use below $\mathbf{x}^{(i)} = (x^{(i)}, y^{(i)}, z^{(i)})$. Eqs. (2.2)–(2.4) are written in matrix form as

$$\mathbf{T} = \mathbf{BF} \quad \text{or} \quad B_{IJ} F_J = T_I, \quad I = 1, 2, \ldots, 10, \tag{2.5}$$

where

$$B_{IJ} = \int_\Omega \Phi(I) \Theta(J) \, \mathrm{d}\boldsymbol{\xi} = \sum_{j=1}^N \Phi(I) \Theta(J) \frac{m_j}{\rho_j}, \tag{2.6}$$

$$\begin{aligned}
&\Phi(1) = W_{ij}, \quad \Phi(2) = W_{ij,x}, \quad \Phi(3) = W_{ij,y}, \quad \Phi(4) = W_{ij,z}, \quad \Phi(5) = W_{ij,xx}, \\
&\Phi(6) = W_{ij,yy}, \quad \Phi(7) = W_{ij,zz}, \quad \Phi(8) = W_{ij,xy}, \quad \Phi(9) = W_{ij,yz}, \quad \Phi(10) = W_{ij,xz},
\end{aligned} \tag{2.7}$$

$$\begin{aligned}
&\Theta(1) = 1, \quad \Theta(2) = x^{(j)} - x^{(i)}, \quad \Theta(3) = y^{(j)} - y^{(i)}, \quad \Theta(4) = z^{(j)} - z^{(i)}, \quad \Theta(5) = \frac{1}{2}(x^{(j)} - x^{(i)})^2, \\
&\Theta(6) = \frac{1}{2}(y^{(j)} - y^{(i)})^2, \quad \Theta(7) = \frac{1}{2}(z^{(j)} - z^{(i)})^2, \quad \Theta(8) = (x^{(j)} - x^{(i)})(y^{(j)} - y^{(i)}), \\
&\Theta(9) = (y^{(j)} - y^{(i)})(z^{(j)} - z^{(i)}), \quad \Theta(10) = (x^{(j)} - x^{(i)})(z^{(j)} - z^{(i)}),
\end{aligned} \tag{2.8}$$

$$F = \{f_i, f_{xi}, f_{yi}, f_{zi}, f_{xxi}, f_{yyi}, f_{zzi}, f_{xyi}, f_{yzi}, f_{zxi}\}^{\mathrm{T}}, \tag{2.9}$$

$$T_I = \int_\Omega f(\xi)\Phi(I)\,\mathrm{d}\xi = \sum_{j=1}^N f_j \Phi(I) \frac{m_j}{\rho_j}, \tag{2.10}$$

$$W_{ij} = W(\mathbf{x}^{(i)} - \boldsymbol{\xi}^{(j)}, h), \quad W_{ij,x} = \left.\frac{\partial W}{\partial x}\right|_{\mathbf{x}=\mathbf{x}^{(i)}, \boldsymbol{\xi}=\boldsymbol{\xi}^{(j)}}. \tag{2.11}$$

Furthermore, m_j and ρ_j denote, respectively, the mass and the mass density assigned to the particle located at the point $\mathbf{x}^{(j)}$. Linear equation (2.5) can be solved simultaneously for $F_1, F_2, \ldots, F_{10}$. It is obvious that the truncation error in Eq. (2.1) is of the order $|\boldsymbol{\xi} - \mathbf{x}^{(i)}|^3$. We named this method of estimating the value of f at a point as the modified SPH (MSPH) method [12]. The function evaluation is second-order consistent, and the first and the second derivatives are first-order and zeroth-order consistent, respectively.

For a one-dimensional problem, Eq. (2.5) reduces to

$$\begin{bmatrix} B_{11} & B_{12} & B_{13} \\ B_{21} & B_{22} & B_{23} \\ B_{31} & B_{32} & B_{33} \end{bmatrix} \begin{Bmatrix} f_i \\ f_{xi} \\ f_{xxi} \end{Bmatrix} = \begin{Bmatrix} T_1 \\ T_2 \\ T_3 \end{Bmatrix}, \tag{2.12}$$

where

$$B_{11} = \sum_{j=1}^N W_{ij} \frac{m_j}{\rho_j}, \quad B_{12} = \sum_{j=1}^N (x^{(j)} - x^{(i)}) W_{ij} \frac{m_j}{\rho_j}, \quad B_{13} = \frac{1}{2} \sum_{j=1}^N (x^{(j)} - x^{(i)})^2 W_{ij} \frac{m_j}{\rho_j},$$

$$B_{21} = \sum_{j=1}^N W_{ij,x} \frac{m_j}{\rho_j}, \quad B_{22} = \sum_{j=1}^N (x^{(j)} - x^{(i)}) W_{ij,x} \frac{m_j}{\rho_j}, \quad B_{23} = \frac{1}{2} \sum_{j=1}^N (x^{(j)} - x^{(i)})^2 W_{ij,x} \frac{m_j}{\rho_j}, \tag{2.13}$$

$$B_{31} = \sum_{j=1}^N W_{ij,xx} \frac{m_j}{\rho_j}, \quad B_{32} = \sum_{j=1}^N (x^{(j)} - x^{(i)}) W_{ij,xx} \frac{m_j}{\rho_j}, \quad B_{33} = \frac{1}{2} \sum_{j=1}^N (x^{(j)} - x^{(i)})^2 W_{ij,xx} \frac{m_j}{\rho_j},$$

$$T_1 = \sum_{j=1}^N f_j W_{ij} \frac{m_j}{\rho_j}, \quad T_2 = \sum_{j=1}^N f_j W_{ij,x} \frac{m_j}{\rho_j}, \quad T_3 = \sum_{j=1}^N f_j W_{ij,xx} \frac{m_j}{\rho_j}, \tag{2.14}$$

N equals the number of particles in the neighborhood of $x^{(i)}$ where the kernel function is positive.

For a one-dimensional problem, we use the kernel function $W(x - \xi, h)$ given by

$$W(x - \xi, h) = \begin{cases} 1.35744 \frac{1}{h\sqrt{\pi}} [1 - ((x - \xi)/2h)^2]^3 \mathrm{e}^{-(x-\xi)^2/h^2}, & |x - \xi| \leqslant 2h, \\ 0, & |x - \xi| > 2h. \end{cases} \tag{2.15}$$

The function $W(x - \xi, h)$ and its first two derivatives are continuous at $|x - \xi| = 2h$. It has a compact support of length $4h$ and the area under the curve $W(x, h)$ vs. x equals 1.

3. Analysis of ASBs

3.1. Problem formulation

We consider simple shearing deformations of a block of an elasto-thermo-viscoplastic material that lies between the planes $y = \pm H$. Thus only the x-velocity is non-zero. Equations governing deformations of the body are [3,4]

$$\rho\dot{v} = s_{,y}, \tag{3.1}$$

$$\rho\dot{e} = -q_{,y} + sv_{,y}, \tag{3.2}$$

$$\dot{\gamma} = v_{,y}, \tag{3.3}$$

$$\dot{\gamma} = \dot{\gamma}_e + \dot{\gamma}_p, \tag{3.4}$$

$$q = -\kappa\theta_{,y}, \tag{3.5}$$

$$\dot{s} = \mu\dot{\gamma}_e, \tag{3.6}$$

$$\rho\dot{e} = \rho c\dot{\theta} + s\dot{\gamma}_e, \tag{3.7}$$

$$\dot{\gamma}_p = \Lambda s, \tag{3.8}$$

$$k\dot{\psi} = s\dot{\gamma}_p, \quad k = k_0\left(1 + \frac{\psi}{\psi_0}\right)^n, \tag{3.9}$$

$$\Lambda = \max\left\{0, \left(\left(\frac{s}{k_0(1-a\theta)\left(1+\frac{\psi}{\psi_0}\right)^n}\right)^{1/m} - 1\right)\bigg/bs\right\}. \tag{3.10}$$

Here a superimposed dot indicates the material time derivative, ρ is the mass density, v the particle x-velocity, s the shear stress, q the heat flux, γ the shear strain, γ_e the elastic shear strain, γ_p the plastic shear strain, θ the temperature rise, e the specific internal energy, κ the thermal conductivity, c the specific heat, ψ an internal variable, μ the shear modulus, k describes the work hardening of the material, a is the thermal softening parameter, b and m are the strain-rate hardening parameters, ψ_0 and n are the work hardening parameters, and k_0 is the yield stress in a quasi-static isothermal simple shear test. The plastic multiplier Λ is zero for elastic deformations and positive for plastic deformations.

Eqs. (3.1) and (3.2) express, respectively, the balance of linear momentum and the balance of internal energy. Eq. (3.3) defines the shear strain rate, (3.4) states the additive decomposition of the total shear strain rate into elastic and plastic parts, (3.5) is Fourier's law of heat conduction, and Eqs. (3.6) and (3.7) are constitutive relations. Eq. (3.8) is the flow rule where the plastic multiplier is given by Eq. (3.10). The work hardening of the material due to plastic deformations is described by Eq. (3.9). When the material is deforming plastically, the yield surface defined by Eq. (3.10) is

$$s = k_0(1-a\theta)\left(1 + \frac{\psi}{\psi_0}\right)^n(1 + b\dot{\gamma}_p)^m. \tag{3.11}$$

Thus the radius of the yield surface increases due to strain- and strain-rate hardening and decreases due to thermal softening.

We nondimensionalize variables as follows:

$$y = H\bar{y}, \quad \gamma = \bar{\gamma}, \quad \psi = \bar{\psi}, \quad v = H\dot{\gamma}_0\bar{v}, \quad t = \frac{\bar{t}}{\dot{\gamma}_0},$$

$$s = k_0\bar{s}, \quad k = k_0\bar{k}, \quad \Lambda = \frac{\dot{\gamma}_0}{k_0}\bar{\Lambda}, \quad b = \frac{\bar{b}}{\dot{\gamma}_0}, \quad \mu = k_0\bar{\mu}, \tag{3.12}$$

$$\theta = \frac{k_0}{\rho c}\bar{\theta}, \quad \rho = \frac{k_0}{H^2\dot{\gamma}_0^2}\bar{\rho}, \quad \kappa = \rho c\dot{\gamma}_0 H^2\bar{\kappa}, \quad a = \frac{\rho c}{k_0}\bar{a}.$$

Here variables with an overbar are nondimensional, $2H$ is the height of the specimen, and $\dot{\gamma}_0$ is the average strain rate.

Substituting the nondimensional variables in Eqs. (3.1)–(3.10), and dropping the overbars, we get

$$\dot{v} = \frac{1}{\rho}s_{,y}, \tag{3.13}$$

$$\dot{\theta} = \kappa\theta_{,yy} + \Lambda s^2, \tag{3.14}$$

$$\dot{s} = \mu(v_{,y} - \Lambda s), \tag{3.15}$$

$$\dot{\psi} = \frac{\Lambda s^2}{\left(1 + \frac{\psi}{\psi_0}\right)^n}, \tag{3.16}$$

$$\Lambda = \max\left\{0, \left(\left(\frac{s}{(1 - a\theta)\left(1 + \frac{\psi}{\psi_0}\right)^n}\right)^{1/m} - 1\right) \Big/ bs\right\}. \tag{3.17}$$

We assume that a homogeneous solution of Eqs. (3.13)–(3.17) under boundary conditions

$$v(-1, t) = -1, \quad v(1, t) = 1, \quad \theta_{,y}(\pm 1, t) = 0, \tag{3.18}$$

is perturbed when $\psi = 0.1$, $\theta = 0.1003$ and $\gamma = 0.0692$, and seek a solution of the resulting initial-boundary-value problem under boundary conditions (3.18) and initial conditions

$$\begin{aligned}
&v(y, 0) = y, \quad \psi(y, 0) = 0.1, \\
&\theta(y, 0) = 0.1003 + 0.1(1 - y^2)^9 e^{-5y^2}, \\
&s(y, 0) = \left(1 + \frac{0.1}{\psi_0}\right)^n (1 - a\theta(y, 0))(1 + b)^m,
\end{aligned} \tag{3.19}$$

where the second term on the right-hand side of the expression for the temperature θ represents a perturbation. The amplitude of the perturbation is large to reduce the computational time required for the deformation to localize at $y = 0$. The peak in the shear stress–shear strain curve occurs at $\gamma = 0.093$. Boundary conditions (3.18)$_3$ imply that the surfaces $y = \pm 1$ are thermally insulated. It is clear that the time is reckoned from the instant of perturbation. Perturbation of the homogeneous solution at different instants only affects the computational time and other aspects of the computed solution remain unchanged.

Because of boundary conditions (3.18) and initial conditions (3.19), we assume that the solution exhibits following properties:

$$v(-y,t) = -v(y,t), \quad \theta(-y,t) = \theta(y,t),$$
$$\psi(-y,t) = \psi(y,t), \quad s(-y,t) = s(y,t). \tag{3.20}$$

Accordingly, we solve the problem on the domain $[0,1]$ and replace boundary conditions (3.18) by

$$v(0,t) = 0, \quad v(1,t) = 1, \qquad \theta_{,y}(0,t) = 0, \quad \theta_{,y}(1,t) = 0. \tag{3.21}$$

3.2. Application of the MSPH Method

Particles are located on the domain $[0,1]$. Eqs. (3.13)–(3.17) are written at each particle, and quantities on the right-hand sides are replaced by their kernel estimates derived from Eq. (2.12). The result is a system of coupled nonlinear ordinary differential equations (ODEs) which are integrated with respect to time t with subroutine LSODE taken from the package ODEPACK developed by Hindmarsh [14].

In order to satisfy symmetry conditions (3.20) and boundary conditions (3.21), we placed several ghost particles with index $I = -1, -2, -3, \ldots$ and $y_{-1} = -y_1$, $y_{-2} = -y_2$, etc. During each time step, the physical quantities at these ghost particles were not computed but were set according to Eq. (3.20). When computing the kernel estimates of derivatives at particles $1, 2, \ldots$, we should consider also particles in the domain $y < 0$ because some of them lie in the support of the kernel for particles $1, 2, \ldots$ Boundary conditions $(3.21)_1$ and $(3.21)_2$ are satisfied by setting $\dot{v} = 0$ for particles located at $y = 0$ and $y = 1$.

Results presented below were obtained by setting MF = 20, ATOL = 1×10^{-7} and RTOL = 1×10^{-7} in LSODE. The parameter MF determines whether the Gear or the Adams–Moulton method is used, and ATOL and RTOL equal, respectively, the absolute and the relative tolerances in the solution. The subroutine adjusts the time step size and the order of the method in order to compute the solution within the prescribed accuracy.

In the numerical solution of the problem, we assigned following values to nondimensional parameters:

$$\rho = 3.928 \times 10^{-5}, \quad \mu = 240.3, \quad a = 0.4973, \quad n = 0.09,$$
$$k = 3.978 \times 10^{-3}, \quad \psi_0 = 0.017, \quad m = 0.025, \quad b = 5 \times 10^6. \tag{3.22}$$

Except for the thermal softening coefficient a, these values are for a typical steel when the average strain rate is 500 s^{-1} and the value of a is enhanced to reduce the computational time; however, we will conduct parametric studies to delineate the effect of a. The temperature rise in °C is obtained by multiplying the corresponding nondimensional value by 89.6. We have set $H = 2.58$ mm.

In the absence of an analytical solution of the problem defined by Eqs. (3.13)–(3.19) a reference numerical solution was computed by the FE code developed by Batra and Kim [4]. Three nonuniform meshes with nodal coordinates given by

$$y_n = \left(\frac{n-1}{200}\right)^p, \quad n = 1, 2, \ldots, 201, \quad p = 3, 4, 5, \tag{3.23}$$

were employed and the following error measure, η, was computed.

$$\eta(y,t) = \frac{s(y,t) - \bar{s}(y,t)}{\bar{s}(y,t)}, \quad \eta_0 = \sup_{\substack{0 \leqslant y \leqslant 1 \\ 0 \leqslant t \leqslant T}} |\eta(y,t)|, \tag{3.24}$$

where $\bar{s}$ is the FE solution computed with $p = 5$ in Eq. (3.23), and $T = 61$ μs. For $p = 3$, 4 and 5, the ASB initiated at $t = 60.55$ μs, as indicated by a catastrophic drop in the shear stress at $y = 0$. Thus T equals the time after the shear band has initiated. Values of η_0 for $p = 3$ and 4 equalled 0.00887 and 0.00607,

respectively, signifying the convergence of the numerical solution. Henceforth, the numerical solution obtained with $p = 5$ is taken as the reference solution against which solutions computed with the MSPH method are compared.

For the MSPH method, the following four distributions of particles were considered:

$$198 \text{ particles}: \quad \Delta y_I = \begin{cases} 6.0 \times 10^{-5}, & 1 \leqslant I \leqslant 50, \\ 1.05 \Delta y_{I-1}, & 50 < I < 170, \\ 2.0 \times 10^{-2}, & 170 \leqslant I \leqslant 198. \end{cases}$$

$$267 \text{ particles}: \quad \Delta y_I = \begin{cases} 4.0 \times 10^{-5}, & 1 \leqslant I \leqslant 75, \\ 1.05 \Delta y_{I-1}, & 75 < I < 190, \\ 1.0 \times 10^{-2}, & 190 \leqslant I \leqslant 267. \end{cases}$$

$$354 \text{ particles}: \quad \Delta y_I = \begin{cases} 3.0 \times 10^{-5}, & 1 \leqslant I \leqslant 100, \\ 1.05 \Delta y_{I-1}, & 100 < I < 210, \\ 6.0 \times 10^{-3}, & 210 \leqslant I \leqslant 354. \end{cases}$$

$$442 \text{ particles}: \quad \Delta y_I = \begin{cases} 2.0 \times 10^{-5}, & 1 \leqslant I \leqslant 150, \\ 1.05 \Delta y_{I-1}, & 150 < I < 264, \\ 5.0 \times 10^{-3}, & 264 \leqslant I \leqslant 442. \end{cases}$$

(3.25)

In each case, the region near $y = 0$ is finely discretized as was also the case for the solution by the FEM. Table 1 lists the ASB initiation time and the error in the solution for the four particle distributions and smoothing length $h = 1.5\Delta$ where Δ is the larger of the distance between two particles adjacent to the one located at y_I.

It is clear that with an increase in the number of particles the MSPH solution converges to the reference FE solution.

Fig. 1(a)–(d) gives the spatial distribution of the error in the MSPH solutions at $t = 60.5, 60.6, 60.7, 60.8, 60.9$ and 61 μs. The spatial location of the point of the maximum error η_0 shifts to the right with an increase in the value of time t. It is because the shear stress at $y = 0$ begins to drop rapidly at $t = 60.55$ μs and an unloading elastic wave emanates from $y = 0$ and propagates outwards as shown in Fig. 2(a)–(d). This and results in remaining Figs. discussed in this section have been computed with the MSPH method and 442 particles.

Fig. 2(b) depicts the time history of the evolution of the shear stress s at $y = 0$; the insert in the Fig. shows results for 60.4 μs $\leqslant t \leqslant 61.1$ μs. These plots reveal that the collapse in the shear stress at $y = 0$ occurs during the 0.1 μs time interval starting at 60.56 μs. The beginning of the collapse of the shear stress at $t = 60.56$ μs signifies the initiation of an ASB at that instant. The sudden drop in the shear stress at $y = 0$ results in an elastic unloading (shock) wave that propagates outwards from $y = 0$; this is illustrated by the spatial variations of the shear stress and the particle velocity plotted in Fig. 2(c) and (d). Curves $1, 2, \ldots$ are at 0.1 μs interval beginning at $t = 60.5$ μs. The nondimensional wave speed computed from either of these

Table 1
Error measure and the ASB initiation time for four particle distributions in the MSPH method

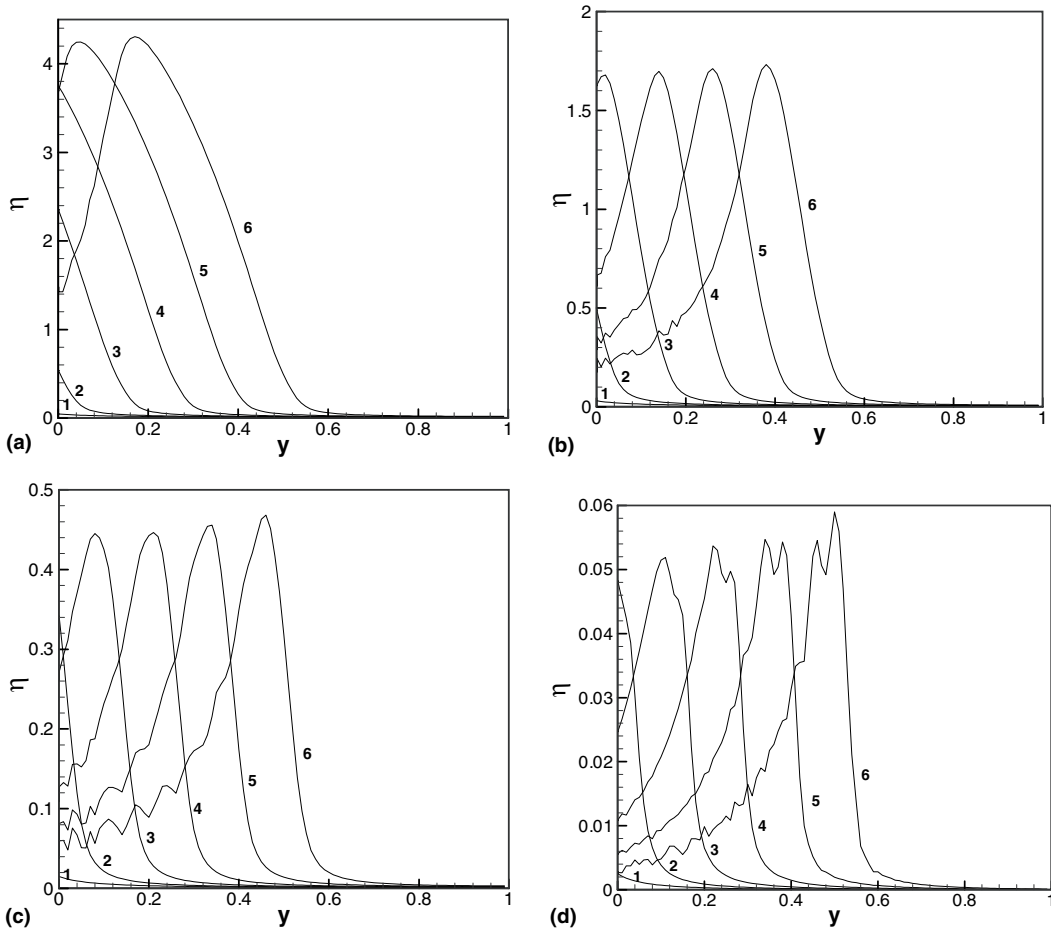| Number of particles	ASB initiation time (μs)	η_0
198	60.88	4.31
267	60.68	1.73
354	60.60	0.468
442	60.56	0.0590
Reference FEM solution	60.55	–

Fig. 1. The spatial distribution of the error in the MSPH solutions at six different times for: (a) 198 particles, (b) 267 particles (c) 354 particles and (d) 442 particles. Curves $1, 2, \ldots, 6$ are at time $t = 60.5, 60.6, \ldots, 61$ μs, respectively.

two plots is 2473 which is very close to $\sqrt{\mu/\rho}$. Furthermore, the change Δv in the particle velocity is related to the jump Δs in the shear stress by

$$\Delta v = \frac{\Delta s}{\rho C},$$

where C is the elastic wave speed. Setting $\Delta s = 1.3$, $\rho = 3.928 \times 10^{-5}$ and $C = 2473$, we get $\Delta v = 13.38$ which agrees with the change in the particle speed computed from results of Fig. 2(d). It takes about 0.81 μs for the wave to travel from $y = 0$ to $y = 1$ from where it is reflected back with a negative value of the shear stress; the reflected wave is labeled as number 11 in these two plots.

The speeds of the unloading elastic wave computed from the MSPH solutions with 198, 267 and 354 particles are 2535, 2502 and 2476, respectively.

Fig. 3(a) shows the spatial distribution of the temperature θ at five different times: $t = 0, 20, 40, 60.5$ and 60.8 μs. For $t \leqslant 60.5$ μs, the temperature rises slowly, and the rate of temperature increase is higher at particles situated near $y = 0$ than at those located away from $y = 0$; a magnified view of the temperature rise near $y = 0$ is given in the insert of Fig. 3(a). It is clear that during the 0.3 μs between $t = 60.5$ μs and

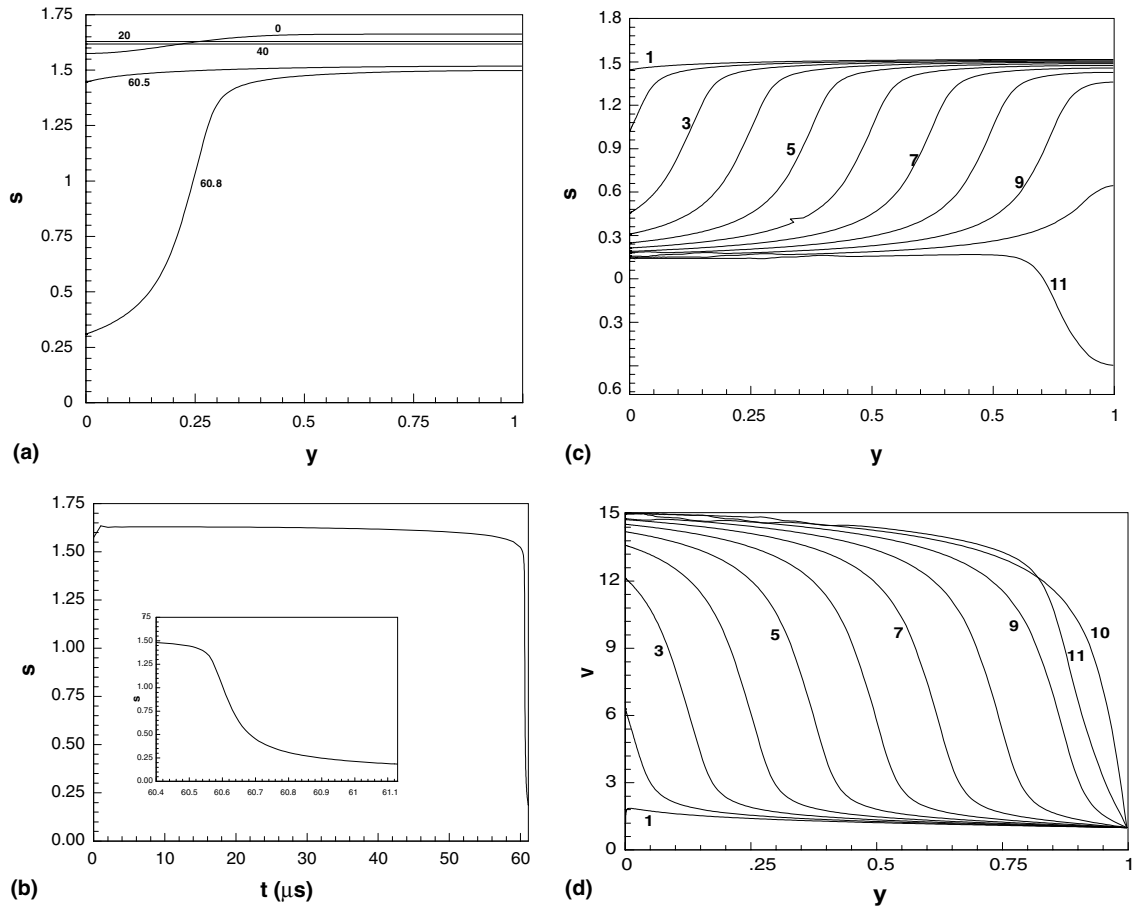Fig. 2. (a) Spatial variation of the shear stress s at five different times: $t = 0, 20, 40, 60.5$ and 60.8 μs. (b) Time history of the shear stress at the specimen center. Spatial variation of (c) the shear stress, and (d) the particle velocity at different times during the localization of the deformation. Curves are plotted at 0.1 μs interval with curve 1 at 60.5 μs.

$t = 60.8$ μs, the temperature at $y = 0$ has risen sharply. During the same time interval, the shear stress that was essentially uniform till $t = 60.5$ μs has dropped precipitously at points close to $y = 0$. Recall that the temperature is high at points where plastic deformations are large. From the plot of the temperature distribution in Fig. 3(a) insert, the width of a shear band is determined to be $2 \times 0.002 \times 2580 = 10.32$ μm which is close to the experimentally determined values of 1–10 μm. There is no unique way of finding the band width either from the experimental or the numerical data. Experimentalists usually determine it from the postmortem data and rarely state how an ASB edge is delineated. Here, the edge of an ASB is assumed to be located at a point where the temperature rise is 40% of the peak value. Identical solutions obtained with $p = 3, 4$ and 5 in (3.23) suggest that 10.32 μm is the converged value of the ASB width.

At first sight it appears that the boundary condition $\theta_{,y}(0,t) = 0$ is not well satisfied by the computed solution. However, magnified plots of the temperature distribution given in Fig. 6(g) suggest that this boundary condition is well satisfied.

Fig. 3(b) evinces the time history of the evolution of the temperature rise at $y = 0$; the insert shows results for 60.4 μs $\leqslant t \leqslant 61.1$ μs. The sudden jump in the rate of increase of temperature at $t = 60.56$ μs can also be taken as a criterion for the ASB initiation.
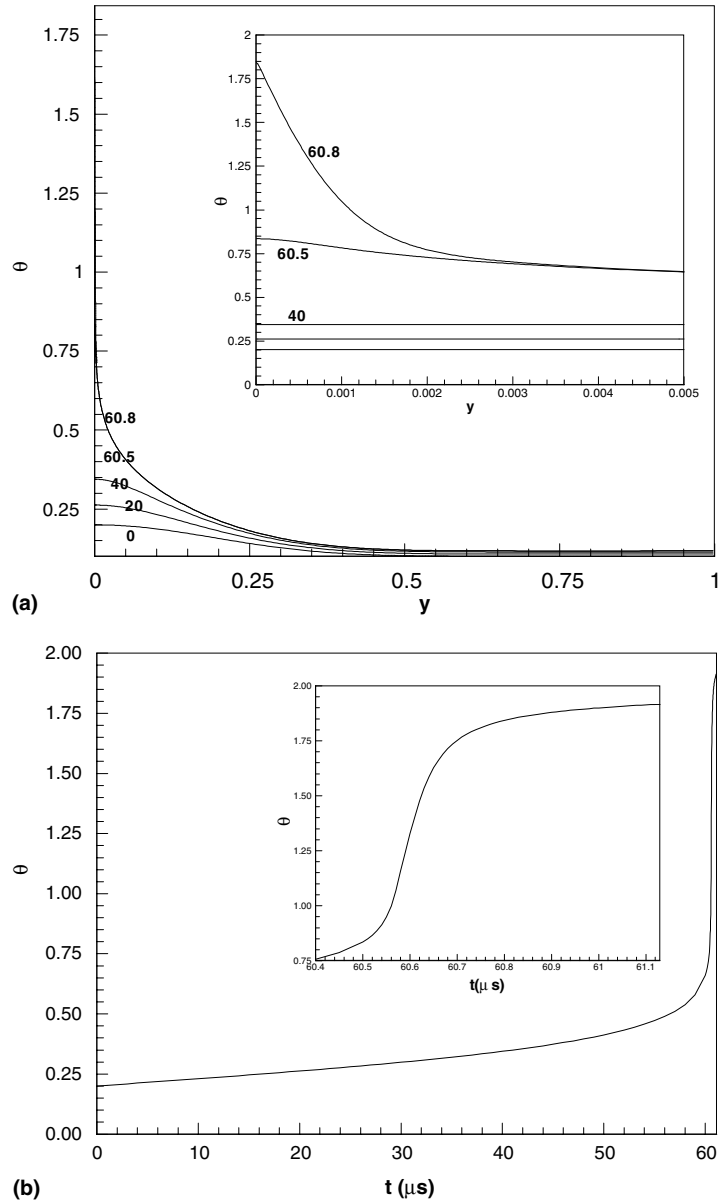
Fig. 3. (a) Spatial variation of the temperature rise at $t = 0, 20, 40, 60.5$ and 60.8 μs. (b) Time history of the temperature rise at the specimen center.

3.3. Effect of the smoothing length h

Fig. 4 exhibits the spatial distribution of the error at six times for $h = \Delta$. A comparison of results plotted in Figs. 4 and 1(d) suggests that $h = 1.0\Delta$ gives lower values of η and hence better numerical solution. For the matrix B in Eq. (2.12) to be invertible, a minimum of three particles must lie in the support of a particle. For $h = 0.75\Delta$, the boundary particle has only two particles in its support. Thus $h < \Delta$ was not attempted.
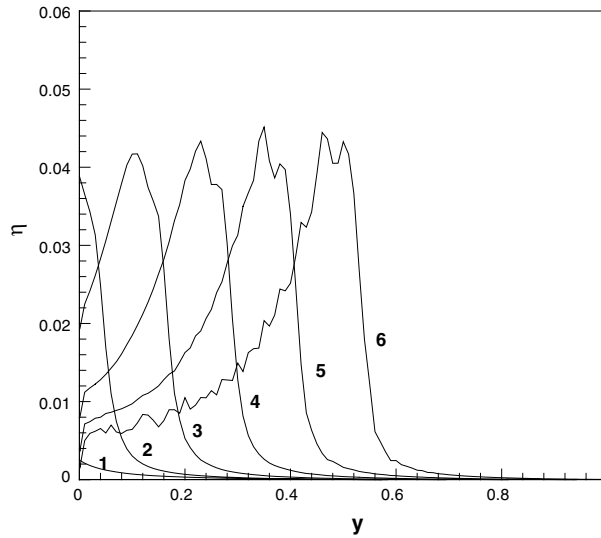
Fig. 4. At six different times the spatial distribution of the error η for $h = 1.5\Delta$. Curves $1, 2, \ldots, 6$ are at $t = 60.5, 60.6, \ldots, 61$ µs, respectively.

These numerical experiments suggest that $h = 1.5\Delta$ gives acceptable results but $h = 1.0\Delta$ yields a slightly lower error η in the numerical solution.

3.4. Choice of the kernel function

We note that the modified quartic spline kernel function

$$W(d, h) = \begin{cases} (1 - d^2)^3(1 - 6d^2 + 8d^3 - 3d^4), & d \leqslant 1, \\ 0, & d > 1, \end{cases}$$

where

$$d = \frac{|x - \xi|}{2h}$$

did not give satisfactory results. It thus is not clear if a kernel function other than that given by (2.15) will yield a good solution.

For the kernel function

$$W(x - \xi, h) = \begin{cases} 1.04823 \frac{1}{h\sqrt{\pi}} \left(e^{(x-\xi)^2/h^2} - e^{-4} \right), & |x - \xi| \leqslant 2h, \\ 0, & |x - \xi| > 2h, \end{cases} \tag{3.26}$$

$h = 1.5\Delta$, and 442 particles, Fig. 5 exhibits the spatial distribution of the error function η at the same times as in Fig. 1(d). The comparison of plots in Figs. 5 and 1(d) suggests that the two kernel functions (3.26) and (2.15) give essentially identical results. Furthermore, the shear band initiation times computed with the two kernels are also the same. Whereas the derivatives of the kernel function (3.26) at $|x - \xi| = 2h$ are discontinuous, those of (2.15) are continuous.
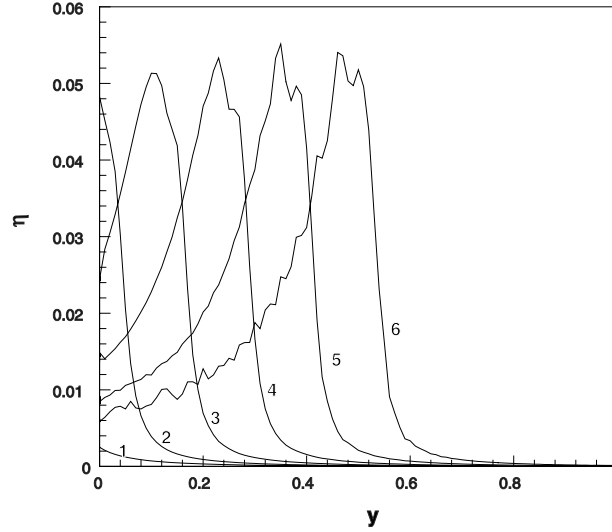
Fig. 5. Spatial distribution of the error in the MSPH solution at time $t = 60.5$ (curve 1), $60.6, \ldots, 61$ μs (curve 6) computed with the kernel function (3.26).

3.5. Post-localization response

Fig. 6(a)–(g) evinces at different times the spatial distribution of the particle velocity v, the work hardening parameter ψ, the plastic strain rate $\dot{\gamma}_p$, the plastic strain γ_p, the shear stress s, and the temperature rise θ within the region where the deformation has localized. The curve 1 is at $t = 60.5$ μs, and curves $2, 3, \ldots$ are at $60.6, 60.7, \ldots$ μs, respectively. Marchand and Duffy [13] performed high strain rate torsional tests on thin-walled tubes and observed that the shear stress collapsed and the plastic strain reached almost 20 in a shear band. Also, a shear band was followed by a crack. In the absence of a fracture criterion, it is hard to ascertain when the material in our computations will fail. In the plots of the particle velocity and the effective plastic strain, curve 8 is different from the remaining 10 curves. The spatial distributions of the shear stress and the temperature rise suggest that computations are stable and numerical results are reasonable. To understand the solution depicted by curve 8, we note that Eqs. (3.8) and (3.10) give

$$\mathrm{d}\dot{\gamma}_p = \frac{(1/b + \dot{\gamma}_p)}{m} \left(\frac{\mathrm{d}s}{s} + \frac{\mathrm{d}\theta}{(1/a) - \theta} - \frac{\mathrm{d}\psi}{(\psi_0 + \psi)/n} \right). \tag{3.27}$$

For $t \simeq 61$ μs, $(1/a) - \theta \simeq 0.1$, $s \simeq 0.2$, $(\psi_0 + \psi)/n \simeq 250$, so there is a competition between the first two terms. Since at $y = 0$, $\mathrm{d}s < 0$ and $\mathrm{d}\theta > 0$, $\mathrm{d}\dot{\gamma}_p$ can become negative. Note that the code correctly gives $\dot{\gamma}_p = 0$ at $y = 0$ and $t = 61.2$ μs, implying thereby that the particle at $y = 0$ is momentarily deforming elastically. With no heat generated at $y = 0$ but heat conducted away from it, $\mathrm{d}\theta < 0$ at $y = 0$ when t is increased from 60.2 to 60.3 μs. $\dot{\gamma}_p = 0$ instantaneously eliminates the effect of strain-rate hardening and reduces the radius of the yield surface to the extent that the material particle deforms plastically at the next instant. For the next two time increments of 0.1 μs each, there is no elastic unloading. When $\dot{\gamma}_p$ at $y = 0$ equals zero, $\dot{\gamma}_p \simeq 3.6 \times 10^5$ at $y = 6 \times 10^{-5}$ since this point is still deforming plastically.

Parametric studies were conducted to delineate the effect of the thermal softening parameter a in Eq. (3.11). Results computed for $a = 0.1, 0.15, 0.2$ and 0.25 indicated that for $a = 0.25$ and 0.2, the drop in the shear stress was catastrophic enough for the elastic unloading wave to emanate from the center of the ASB and propagate outwards with the elastic shear wave speed. However, for $a = 0.15$ and 0.1 the shear stress
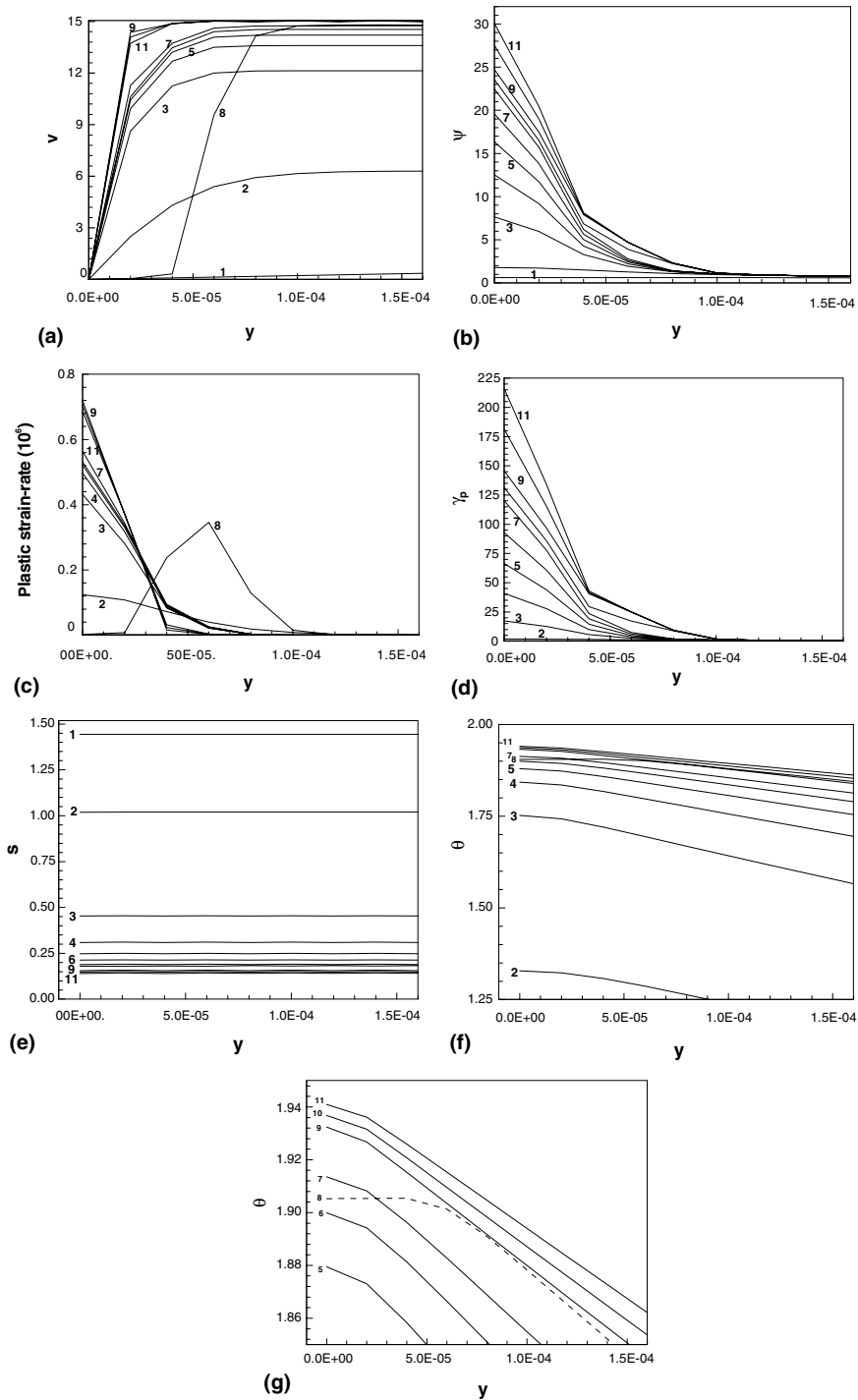
Fig. 6. Spatial variation at different times during the localization of the deformation of: (a) the particle velocity, (b) the work-hardening parameter, (c) the plastic strain-rate, (d) the plastic strain, (e) the shear stress, (f) the temperature and (g) the temperature with magnified vertical scale. Curve 1 is at $t = 60.5$ μs, curve 2 at 60.6 μs, etc.

did not decrease rapidly enough for an elastic unloading wave to emanate from $y = 0$. For $a = 0.1$, all curves in Fig. 6(c) looked alike. Results plotted in Fig. 7 reveal that the initiation time of an ASB decreases exponentially with an increase in the value of a. A least squares fit to the computed values is

$$t_{\text{ASB}} = 10^{\alpha} \ \mu\text{s}, \quad \alpha = 3.4\text{e}^{-1.27a}, \tag{3.28}$$

where t_{ASB} is the ASB initiation time.

3.6. Comparison of results from the MSPH, FE and pseudo-spectral methods

Bayliss et al. [15] have analyzed a one-dimensional ASB problem, similar to the one studied herein, by a pseudo-spectral method. Whereas we have modeled thermal softening by an affine function of temperature rise, they used an exponential function. We have incorporated the exponential thermal softening function in our FE and MSPH codes. The FE and the MSPH results are compared with those of Bayliss et al. [15] in Table 2 and Fig. 8. In each case the defect is modeled by a slightly weaker material near $y = 0$. Values of material and geometric parameters, and the defect size and type are given in [15]. Times t_1, t_2, t_3 and t_4 equal, respectively, when $\dot{\gamma}_{\text{p}}$ at $y = 0$ is maximum, $\dot{\gamma}_{\text{p}}$ at $y = 0$ has dropped to approximately 40% of its peak value, the shear stress at $y = 0$ is maximum, and the temperature at $y = 0$ attains a minimum after having
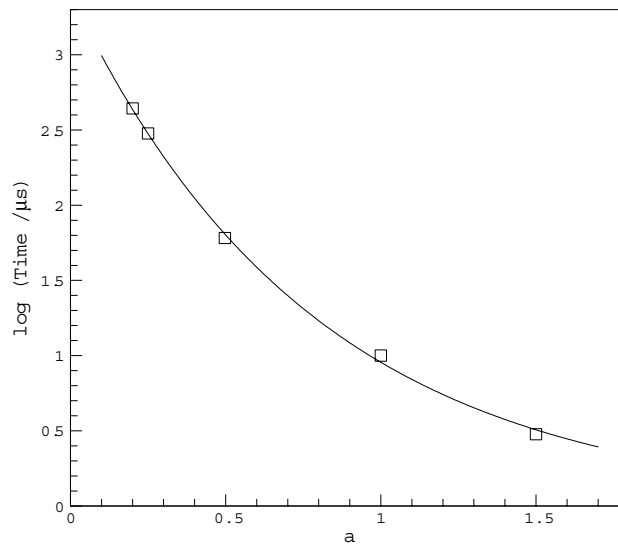

Fig. 7. Variation of the shear band initiation time with the non-dimensional thermal softening coefficient a. Centers of squares are data points and the solid curve is the least squares fit.

Table 2
Comparison of results from the pseudo-spectral, MSPH and FEM methods

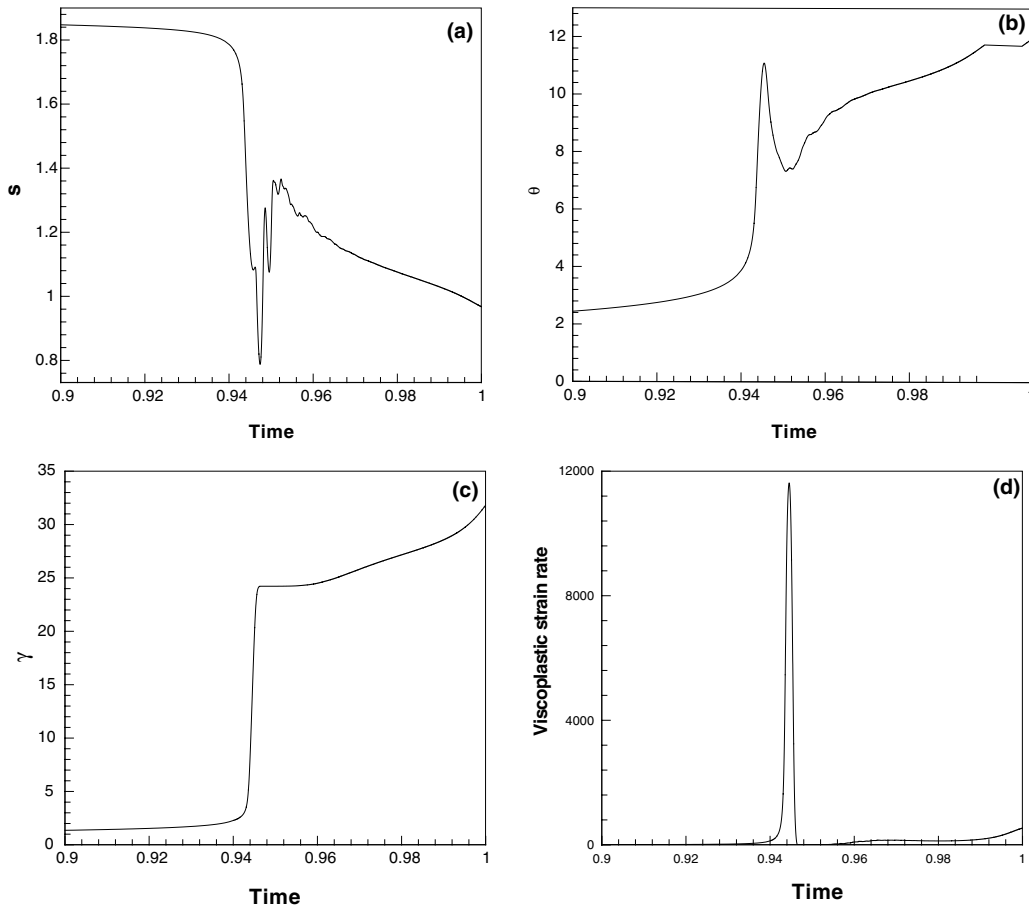| Time	Pseudo-spectral	MSPH	FEM
t_1	0.7239	0.9445	0.9446
t_2	0.7252	0.9455	0.9456
t_3	0.7268	0.9505	0.9507
t_4	0.7248	0.9474	0.9475

Fig. 8. Time histories at $y = 0$ of the shear stress, the temperature rise, the plastic strain and the plastic strain rate computed with the MSPH method for the problem studied by Bayliss et al. [15].

peaked. Fig. 8 depicts the time histories of s, θ, γ_p and $\dot{\gamma}_p$ at $y = 0$. Solutions computed with the MSPH and the FE methods were virtually identical; thus only the MSPH solution is shown. A comparison of these plots with those in Fig. 1 of [15] reveals that all three methods give results very close to one another. The intermediate peak values, at $y = 0$ and $t \simeq 0.94$, of the temperature rise, the plastic strain and the plastic strain rate computed with the MSPH (the pseudo-spectral) method equal respectively 11 (9), 24 (13) and 11,500 (5300). Whereas peak values of θ, γ_p and $\dot{\gamma}_p$ obtained with the MSPH method are higher than those with the pseudospectral method, that of the shear stress is $\simeq 1.84$ for the two methods. Differences in the values of $t_2 - t_1$, $t_3 - t_1$ and $t_4 - t_1$ could be due to the different peak values attained by s, θ, γ_p and $\dot{\gamma}_p$. It is not clear why the value of t_1 for the MSPH and the FE solutions is higher than that for the solution by the pseudo-spectral method.

3.7. Remarks

For the simple shearing problem, the FEM gives good results since the Lagrangian FE mesh is not distorted and the smallest element size of 10^{-7} enables one to capture strains of 10 and higher. For

two-dimensional problems, one can still use a Lagrange FE mesh but not so small elements. Furthermore, the mapping from an element in the reference configuration to that in the present configuration can become singular or the element can get extremely distorted and the time step for stable integration of the ODEs is diminished to so small a value that computations cannot be performed in a reasonable CPU time. For the simple shearing problem, the distance between two nodes stays fixed so computations proceed at a reasonable pace even when strains become large. In the MSPH, no nodal connectivity is needed. The expectation is that satisfactory results can be computed with the MSPH for two- and three-dimensional problems.

Table 3 compares the FE and the MSPH methods.

For the one-dimensional ASB problem studied herein the manual time required to prepare the input file is the same for the FE and the MSPH methods. Since the FEM requires considerably less CPU time than the MSPH method, it should be used. However, for the two-dimensional shear band problem in an inhomogeneous body with the point where an ASB initiates unknown a priori, a satisfactory resolution of the ASB will require that the FE mesh be refined adaptively; e.g. see [16]. However, each refinement of the mesh smoothens out deformation fields and tends to delay the ASB initiation time. Also intense plastic deformations within the shear banded region will significantly distort the Lagrangean mesh. For such problems, the MSPH method may be advantageous over the FEM. One will gain accuracy at the cost of CPU time.

In the solution of Eq. (3.14) by the MSPH method, $\theta_{,yy}$ at a particle is approximated by Eq. (2.12) which may not be very good because only three terms are retained in the Taylor series expansion (2.1). The situation is similar to that in the FEM employing polynomial basis functions of degree one. For the present problem, the effect of thermal conductivity prior to the initiation of an ASB is negligible (e.g. see [17]).

Table 3
Comparison of the MSPH and the FE methods for an elastodynamic problem

	MSPH	FE
Nodal connectivity	Not required	Required
Assembly of equations	Not required	Required
Weak form	None	Global
Subdomains (two-dimensional problem)	None	Polygonal and disjoint
Basis functions	Complex and difficult to express in closed form	Simple polynomials
Satisfaction of essential boundary conditions	Requires extra effort	Easy to enforce
Satisfaction of natural boundary conditions	Requires additional effort	Included in the weak formulation
Stiffness matrix	Asymmetric, large band width that cannot be determined a priori, not necessarily positive semidefinite	Symmetric, banded, stiffness matrix positive definite after imposition of essential boundary conditions
Mass matrix	Diagonal, positive-definite	Symmetric, banded, positive definite
Sum of elements of mass matrix	Not necessarily equal to the total mass of the body	Equals total mass of the body
Stresses/strains	Smooth everywhere	Good at integration points
Addition of nodes	Easy	Difficult
Determination of time step size for stability in an explicit algorithm	Difficult, requires determination of the maximum frequency of the structure	Relatively easy
Computation of the total strain energy of the body	Difficult	Relatively easy
Data preparation effort	Little	Extensive
CPU time for the ASB problem (201 nodes for FEM, 442 particles for MSPH)	≃6 h	≃0.5 h

4. Conclusions

We have used the MSPH method to analyze simple shearing deformations of an elasto-thermo-visco-plastic body. The effects of elastic unloading, strain-hardening, strain-rate hardening, thermal softening, heat conduction and inertia forces are considered. Equal and opposite velocity is prescribed on the two thermally insulated bounding surfaces of the block. When a perturbation near the center of the block is introduced in the homogeneous solution of the governing equations, the deformation localizes into a narrow region of intense plastic deformation with peak plastic strains of 20. The width of the intensely deformed region is only 10.3 μm. Computed results agree well with those obtained by the finite element method. In all three cases particles or nodes are placed nonuniformly with the distance between adjacent nodes increasing gradually as one moves away from the center of the block.

For the one-dimensional wave propagation in a bar, two-dimensional transient heat conduction, and the one-dimensional transient thermo-elasto-viscoplastic problem, the MSPH method with the exponential kernel function and the smoothing length equal to the distance between two adjacent particles gives results that agree well with either the analytical solution or the converged FE solution.

In view of the noticeably more CPU time needed for the MSPH method than that for the FE solution, it is recommended that one use the FEM to analyze one-dimensional ASB problem. The data preparation time is virtually the same for the two methods.

References

[1] S.N. Atluri, S.P. Shen, The Meshless Local Petrov–Galerkin Method, Tech. Science Press, California, 2002.
[2] G.R. Liu, Mesh Free Methods, CRC Press, Boca Raton, Florida, 2003.
[3] R.C. Batra, The initiation and growth of, and the interaction among, adiabatic shear bands in simple and dipolar materials, Int. J. Plasticity 3 (1987) 75–89.
[4] R.C. Batra, C.H. Kim, Adiabatic shear banding in elastic–viscoplastic nonpolar and dipolar materials, Int. J. Plasticity 6 (1990) 127–141.
[5] L.B. Lucy, A numerical approach to the testing of the fission hypothesis, Astron. J. 82 (1977) 1013.
[6] R.A. Gingold, J.J. Monaghan, Smoothed particle hydrodynamics: theory and application to non-spherical stars, Mon. Not. R. Astron. Soc. 181 (1977) 375–389.
[7] L.D. Libersky, A.G. Petschek, Smoothed particle hydrodynamics with strength of materials, Advances in the mesh free Langrange method, Lecture Notes in Phys. 395 (1990) 248–257.
[8] J.K. Chen, J.E. Beraun, C.J. Jih, An improvement for tensile instability in smoothed particle hydrodynamics, Comput. Mech. 23 (1999) 279–287.
[9] J.K. Chen, J.E. Beraun, C.J. Jih, Completeness of corrective smoothed particle method for linear elastodynamics, Comput. Mech. 24 (1999) 273–285.
[10] P.W. Randles, L.D. Libersky, Normalized SPH with stress points, Int. J. Numer. Methods Eng. 47 (2000) 1445–1462.
[11] R. Vignjevic, J. Campbell, L.D. Libersky, A treatment of zero-energy modes in the smoothed particle hydrodynamics method, Comput. Methods Appl. Mech. Eng. 184 (2000) 67–85.
[12] G.M. Zhang, R.C. Batra, Modified smoothed particle hydrodynamics method and its application to transient problems, Comput. Mech., in press, available online.
[13] A. Marchand, J. Duffy, An experimental study of the formation process of adiabatic shear bands in a structural steel, J. Mech. Phys. Solids 36 (1988) 251–283.

[14] A.C. Hindmarsh, Description and use of LSODE, the Livermore solver for ordinary differential equations, Lawrence Livermore National Laboratory Report UCRL-ID-113855, 1993.

[15] A. Bayliss, T. Belytschko, M. Kulkarni, D.A. Lott-Crumpler, On the dynamics and the role of imperfections for localization in thermo-viscoplastic materials, Modelling Simulat. Mater. Sci. Eng. 2 (1994) 941–964.

[16] R.C. Batra, K.I. Ko, An adaptive mesh refinement technique for the analysis of shear bands in plane strain compression of a thermoviscoplastic solid, Comput. Mech. 10 (1992) 369–379.

[17] R.C. Batra, C.H. Kim, Effect of thermal conductivity on the initiation, growth and band width of adiabatic shear bands, Int. J. Eng. Sci. 29 (1991) 949–960.